Titan-like exoplanets: Variations in geometric albedo and effective transit height with haze production rate

Jade Checlair [1,2 *], Christopher P. McKay[1], and Hiroshi Imanaka[1,3]

[1] *Space Science Division, NASA Ames Research Center, United States*
[2] *Department of Physics, University of Toronto, Canada*
[3] *SETI Institute, United States*

* Corresponding author at: jade.checlair@gmail.com Tel.: +1-647-973-2444
E-mail addresses:
jade.checlair@gmail.com (J. Checlair)
chris.mckay@nasa.gov (C.P. McKay)
himanaka@seti.org (H. Imanaka)

Revised for PSS Feb 2016

Color in print is required.

ABSTRACT

Extensive studies characterizing Titan present an opportunity to study the atmospheric properties of Titan-like exoplanets. Using an existing model of Titan's atmospheric haze, we computed geometric albedo spectra and effective transit height spectra for six values of the haze production rate (zero haze to twice present) over a wide range of wavelengths (0.2-2 um). In the geometric albedo spectra, the slope in the UV-visible changes from blue to red when varying the haze production rate values from zero to twice the current Titan value. This spectral feature is the most effective way to characterize the haze production rates. Methane absorption bands in the visible-NIR compete with the absorbing haze, being more prominent for smaller haze production rates. The effective transit heights probe a region of the atmosphere where the haze and gas are optically thin and thus is not effectively probed by the geometric albedo. The effective transit height decreases smoothly with increasing wavelength, from 376 km to 123 km at 0.2 and 2 um, respectively. When decreasing the haze production rate, the methane absorption bands become more prominent, and the effective transit height decreases with a steeper slope with increasing wavelength. The slope of the geometric albedo in the UV-visible increases smoothly with increasing haze production rate, while the slope of the effective transit height spectra is not sensitive to the haze production rate other than showing a sharp rise when the haze production rate increases from zero. We conclude that geometric albedo spectra provide the most sensitive indicator of the haze production rate and the background Rayleigh gas. Our results suggest that important and complementary information can be obtained from the geometric albedo and motivates improvements in the technology for direct imaging of nearby exoplanets.

KEYWORDS *Titan, Exoplanet transit, Haze, Geometric albedo, Transit height, Atmosphere limb*

1. INTRODUCTION

The detection of numerous exoplanets by the Kepler mission has increased interest in the characterization of planets and moons in other star systems. Characterizing the atmospheres of those new worlds is difficult due to their large distances from the Earth. The transit method for detecting exoplanets is based on observing the transit of the planets across their star. This has naturally led to considerable interest in the use of transit spectroscopy to study exoplanet atmospheres (e.g. Seager and Sasselov 2000, Brown 2001, Hubbard et al. 2001). Direct imaging to obtain the albedo spectra provides an alternative method to study a planet's atmospheric and surface properties (e.g. Cahoy et al. 2010). Recent exoplanet studies based on direct imaging have been reported (Ingraham et al. 2014, Macintosh et al. 2015, Mesa et al. 2015).

The effective transit height spectrum essentially represents the height of the atmosphere of the planet above the solid surface as a function of wavelength. It is determined when the planet is directly in front of the star as viewed from Earth, and is measured by the resulting reduction in starlight. The albedo spectrum is the spectrum of reflected light from the planet, normalized to the light source. This albedo spectrum depends both on the intrinsic reflectivity of the planet and its size. If the planet is not spatially resolved, the albedo is expressed as a geometric albedo referenced to a phase of zero. The light source and the observer are then in a line, as would occur at opposition for worlds of the outer Solar System. If the planet is spatially resolved, the albedo spectrum is usually a nadir spectrum, as for the case of the Earth viewed from orbit. In both cases, the observer is looking in the direction normal to the surface.

The worlds of our Solar System including the Earth are often used as analogs and are observed using the same methods proposed for the study of exoplanets (e.g. Vidal-Madjar et al. 2010, Robinson et al. 2014). Direct imaging of Solar System worlds is possible, and the similarities in the geometries of the occultation of a Solar System world by a star, by the Sun, or by a spacecraft, to an exoplanet transit provide a method for exploring the utility of transit observations. Thus, both albedo and transit studies can be used to relate information on the structure and atmosphere of worlds in the Solar System to potential methods for the study of exoplanets.

Saturn's largest moon, Titan, is of particular interest for this purpose, as it is the only natural satellite to have a dense atmosphere where active chemistry resulted in organic gases and haze. Titan is a small world after all, with a radius 0.4 times Earth but its atmosphere has a surface pressure 50% larger than Earth (Fulchignoni et al. 2005). The atmosphere is composed largely of nitrogen (95%), with methane (5%) and other hydrocarbons present (Niemann et al. 2005). The low gravity and thick atmosphere on Titan result in an atmosphere that is far more extended than Earth's, effectively reaching up to more than half the radius of the solid body (Porco et al. 2005, Fulchignoni et al. 2005).

Perhaps the most interesting characteristic of Titan's atmosphere is the thick high-altitude haze formed of organic aerosols, resulting from the photochemical dissociation of methane and nitrogen. Titan's organic haze has been studied in laboratory simulations (e.g., Khare et al. 1984, McKay 1996, Coll et al., 1999, Imanaka et al. 2004, Szopa et al., 2006, Cable et al., 2011), photochemical models (Yung et al. 1984, Wilson and Atreya 2004, Lavvas et al., 2008) and spacecraft observations by Voyager (Rages et al. 1983, Rages and Pollack 1980) and Cassini-Huyhens (e.g., Tomasko and West, 2009, West et al., 2014). Hazes can dramatically influence atmospheric observations, obscuring deep layers at visible wavelengths. Considering Titan-like exoplanets, it is thus important to understand how these hazes affect the albedo spectra and transit spectra when observing hazy exoplanets (Pont et al. 2008, Lecavalier des Etangs et al. 2008, Sing et al. 2009, Bean et al. 2010, Gibson et al. 2011, Robinson et al. 2014).

In this paper we approach the study of the atmosphere of Titan-like exoplanets by computing the geometric albedo spectra and effective transit height spectra of Titan's atmosphere as a function of haze production rate. This is because haze production rates would be affected by several factors, such as different amounts of incident steller UV flux and methane concentrations. Robinson et al. (2014) produced transit radius spectra of Titan from 1 to 5 um based on Cassini occultation data, and computed a haze model fit to this data from 1 to 3.8 um. They found an effective transit height smoothly varies from 270 to 100 km from 1 to 3.8 um except methane absorption features overlapped on a continuum formed by the haze. However, limited observations by the Cassini VIMS did not allow to explore the transit radius spectra at wavelengths shorter than 1 um. This visible/near IR region might provide crucial information about the characteristic of haze. Here, we consider how different amounts of haze could influence both transit and geometric albedo spectra of Titan-like worlds, with the varying contrast between the haze, scattering by the nitrogen gas, absorption by methane, and the surface reflectivity. We present results for geometric albedo and effective transit height spectra for values of the haze production rate, from zero to twice the present production rate, for a wider range of wavelengths than previous study.

2. ATMOSPHERIC HAZE MODEL

We used the microphysics haze and opacity model developed by McKay et al. (1989). This model was developed to determine the thermal structure of Titan's atmosphere and its results have been largely confirmed by in-situ measurements of temperature and radiative fluxes by the Huygens Probe (Tomasko et al. 2008).

The details of the haze model are described in McKay et al. (1989) and are only briefly summarized here. The haze model assumes steady-state and is based on the assumptions that (1) all the particles at a given altitude are spherical and have the same radius, and (2) only coagulation and sedimentation are considered within homogeneous layers. The haze is produced high in the atmosphere (~600 km) as seed particles small enough (~1 nm) that the initial size does not affect the results, which then experience coagulation to larger sizes and sedimentation through the atmosphere. The basic equations that determine the haze properties with altitude are conservation of mass and number (McKay et al. 1989). The advantages of this simple model over merely specifying particle size and density profiles is that the adjustable parameters in the model can be related to physically meaningful quantities such as the haze production rate, which can then be varied systematically. All other parameters of the microphysics model (aerosol charging, production altitude, particle shape and density) are identical to those used in the baseline case of McKay et al. (1989). Note that the altitude of haze production does not change the haze size or opacity distribution, provided that it is well above the main haze layer (McKay et al. 1989).

The atmosphere temperature and pressure profile used in all calculations is that determined by Fulchignoni et al. (2005), then extended upward to 670 km – the top of the haze model - by an isothermal layer. Any interaction between changes in the haze production rate and changes in the atmosphere temperature profile are neglected.

The optical model of McKay et al. (1989) warrants a more complete description here, as it is key to the computation of the geometric albedo and the transit spectra. The wavelength range covers 0.2 to 2 um with external sunlight (starlight) as the only source. This optical model computes the solar radiation in a series of spectral intervals with vertical resolution. The opacity sources are Rayleigh scattering by the gas (predominantly N_2), absorption by methane, and

scattering and absorption by haze particles. The optical properties of the haze used by McKay et al. are scaled to the laboratory values of Khare et al. (1984) – the imaginary index of refraction used is the Khare et al. value multiplied by 4/3. Rages and Pollack (1980), and more recently Rannou et al. (2010), showed that spacecraft observations of Titan are consistent with scaling the Khare et al. (1984) results up to about 0.8 um with a value approximately constant at 0.01 from 0.8 to 2 um, rather than falling to a value as low as 0.001 as suggested by the laboratory data of Khare et al. (1989). We have modified the optical properties of the model accordingly. The scattering by the haze is computed by Mie scattering and depends on the optical properties and the Mie size parameter. The model is a spherical drop model but measurements and theory indicate that the haze particles are fractal. In the UV this would make the haze darker (Wolf and Toon 2010) increasing the contrast we report here with the Rayleigh gas and increasing the altitude of the effective transit height. However it is not expected that the nature of the dependence with wavelength will change in a qualitative way. We computed the single scattering albedo and asymmetry factor due to the scattering of the haze and gas. Multiple scattering and the scattering asymmetry factor are both important in determining the geometric albedo (McKay et al.). The model can, in principle, also compute the forward scattering peak due to the haze particles. It has been shown that is some cases this can contribute to the transit spectrum but would not be important for the case of multiple scattering as in present Titan (de Kok and Stam 2012). Furthermore, the effect is likely to be small in the UV and visible due to the absorbing nature of the small dark haze particles and the fact that Rayleigh scattering by the gas does not have a forward scattering peak.

To compute the geometric albedo, McKay et al. (1989) use the Eddington source function method as described by Toon et al. (1989), with 10 Gauss point integration over angle. In this method the source function from the Eddington two-stream is used in an exact integral of the radiative transfer equation in order to compute emergent intensities. The radiation reflected from the surface is determined by the two-stream solution. The method works best for an optically thick atmosphere. Toon et al. (1989) present a detailed discussion of the errors associated with the radiative transfer methods.

The haze production rate that currently characterizes Titan's haze was determined by McKay et al. (1989) to be 1.2×10^{-14} g cm^{-2} sec^{-1} (see also McKay et al. 2001) and is used here. We varied the haze production rate in multiples of the current production: 0x, 0.01x, 0.1x, 0.5x, 1x (the present case), and 2x. For each of those values, we computed the geometric albedo values for wavelengths from 0.2 to 2 um to observe the changes in the profile depending on the amount of haze. The haze was treated as a separate parameter, as it was varied without changing other factors such as the temperature profile. Changing the haze production rate would in reality affect those factors, but here we focus on changes due solely to a different amount of haze in the atmosphere. We compare our results for the geometric albedo to the data of Neff et al. (1984) corrected for the size of the optical disk of Titan, and verify that our spectrum for the haze production rate for the 1x case reproduces the previous result of McKay et al. (1989). The McKay et al. (1989) model does not include the methane absorption bands in the 1-2 um region because that study was only interested in the continuum in that wavelength region as a way to sense the lower atmosphere and surface. This region is particularly sensitive to the surface albedo and to properties of the lower atmosphere and clouds. Similarly to McKay et al., we have not added these methane bands as we also use this region as a way to determine how the geometric albedo and effective transit height are sensitive to the lower atmosphere and surface.

The model of McKay et al. (1989) determines values for the vertical optical depths as a function of altitude. We then used those values and the Chapman function to compute the limb optical depths from the vertical optical depth as described below.

The vertical and the limb optical depths can be related using the Chapman function at a $\pi/2$ angle:

$$\tau(h_P) = 2\,\tau_V(h_P)\,Ch\left(X_P,\,\theta_P = \frac{\pi}{2}\right) \quad (1)$$

where h_P is the altitude at the closest point P to the surface of the planet, and $X_P = r_P/H(h = h_P)$ with $r_P = R + h_P$, R being the radius of the planet, $H(h = h_P)$ the scale height at altitude h_P. θ_P is the stellar zenith angle at point P, here it is fixed at $\pi/2$. τ_V is the vertical optical depth at h_P. $\tau(h_P)$ is the limb optical depth along a slant path passing through point P at h_P.
The Chapman function can be approximated as

$$Ch\left(X_p, \frac{\pi}{2}\right) = \left[\frac{\pi}{2}X_p\right]^{1/2} \quad (2)$$

which is valid for planets where $r_p \gg H$.

This problem and its approximation were originally solved by Chapman (1931), who derived a way of computing the column amount of an exponentially distributed atmosphere along any solar zenith angle, including $\pi/2$, correctly accounting for spherical geometry. Smith and Smith (1972) developed a numerical approach accurate to within 2% for all solar zenith angles when the planet radius > 50 times the atmosphere scale height. Similar results were later obtained by Fortney (2005), who geometrically derived the approximate expression for the Chapman function. For planets such as the Earth and Jupiter, those considered by Fortney, the approximate method yields results very close to using the complete function. However, for bodies similar to or smaller than Titan, using the approximation as did Robinson et al. (2014) can result in an error of up to several percent. We opted to use the full version of the Chapman function without any approximation as to obtain the most accurate results. Our approach is described in full in the Appendix.

In principle, determining the effective transit height requires a complex analysis that includes refraction and absorption. Lecavalier des Etangs et al. (2008) suggested a simple method for determining the effective transit height by solving for the optical depth at a certain altitude such that a sharp occulting disk, with radius the sum of the planet radius and the altitude probed, produces the same absorption depth as the planet with its translucent atmosphere. In this approximate method, the effective transit height is that height at which the limb optical depth of the atmosphere becomes equal to 0.56. We use this approach here. As expected, changing the value of this reference limb optical depth changes the effective transit height. (The vertical optical depth as a function of altitude for the 1x case is shown in Figure 3 of McKay et al. 1989). For example, for the 1x case, using 1.0 instead of 0.56 decreases the height by about 20 km. Nonetheless, our conclusions are not sensitive to the precise value assumed here, as the slope of the effective transit height does not vary with this value. For Titan the ratio of the limb optical depth to the vertical optical depth (2 times the Chapman function) is typically about 20, but varies with altitude and hence with wavelength.

The role of refraction is well illustrated by Betremieux and Kaltenegger (2014, Figure 2), who describe refraction's three main effects on the rays passing through a planet's atmosphere. Bellucci et al. (2009) have specifically discussed refraction in the case of stellar occultation for Titan's atmosphere. Refraction is often considered in transit spectroscopy studies mainly because it can deflect rays at certain altitudes away from the observer. This effect depends on the angular size of the parent star with respect to the planet, as for smaller angular sizes, rays come from a

stellar region behind the planet, while for larger angular sizes, rays would need to come from a region larger than the stellar radius to reach the observer (Betremieux and Kaltenegger 2014). This makes probing atmospheric regions at altitudes lower than a certain critical height difficult. However, we note that Misra et al. (2014) have proposed a method that uses refraction occurring prior to ingress and/or subsequent to egress to probe pressures greater than can be probed during transit. We ignore refraction, because the haze is absorbing at altitudes above which refraction becomes important. This is not correct for the case of zero haze, but refraction is less important even in this case due to Titan's low gravity and hence large scale height. Only at the longer wavelengths (1 um and above), when the transit height in the case of zero haze falls below 35 km or so, is the neglect of refraction inaccurate. We also ignore the angular size of the parent star with respect to the planet. As discussed earlier, we ignore the effect of forward scattering (de Kok and Stam, 2012).

Our spectral interval overlaps the results of Robinson et al. (2014) from 1 to 2 um and we can compare our effective transit height with their values. We matched our effective transit height spectrum to theirs by reducing the specific density of the haze material to 0.4 (from 1). We computed the effective transit height spectra for all haze production rates for each value of the specific density of the haze particles.

We determined the slope as a function of wavelength of the geometric albedo and effective transit height spectra at 0.4 um and 0.2 um to determine the sensitivity of the spectrum and their use in characterizing the haze production rate.

3. RESULTS

We obtained geometric albedo spectra for six values of the haze production rate (Figure 1) – 0x, 0.01x, 0.1x, 0.5x, 1x, and 2x the present haze production rate. Each profile was compared to the observed data from Neff et al. (1984) to demonstrate how the spectrum changes with the value of the haze production rate. The spectra were computed for wavelengths from 0.2 to 2 um, thus including more spectral features than with a narrower range of wavelengths. Methane absorption features are not modeled for wavelengths from 1 to 2 um and only the continuum points of the spectra are shown. The specific density of the haze material is kept fixed at 1 as in McKay et al. (1989).

As expected, the 1x profile reproduces the baseline result of McKay et al. (1989) and its features match the data from Neff et al. (1984).

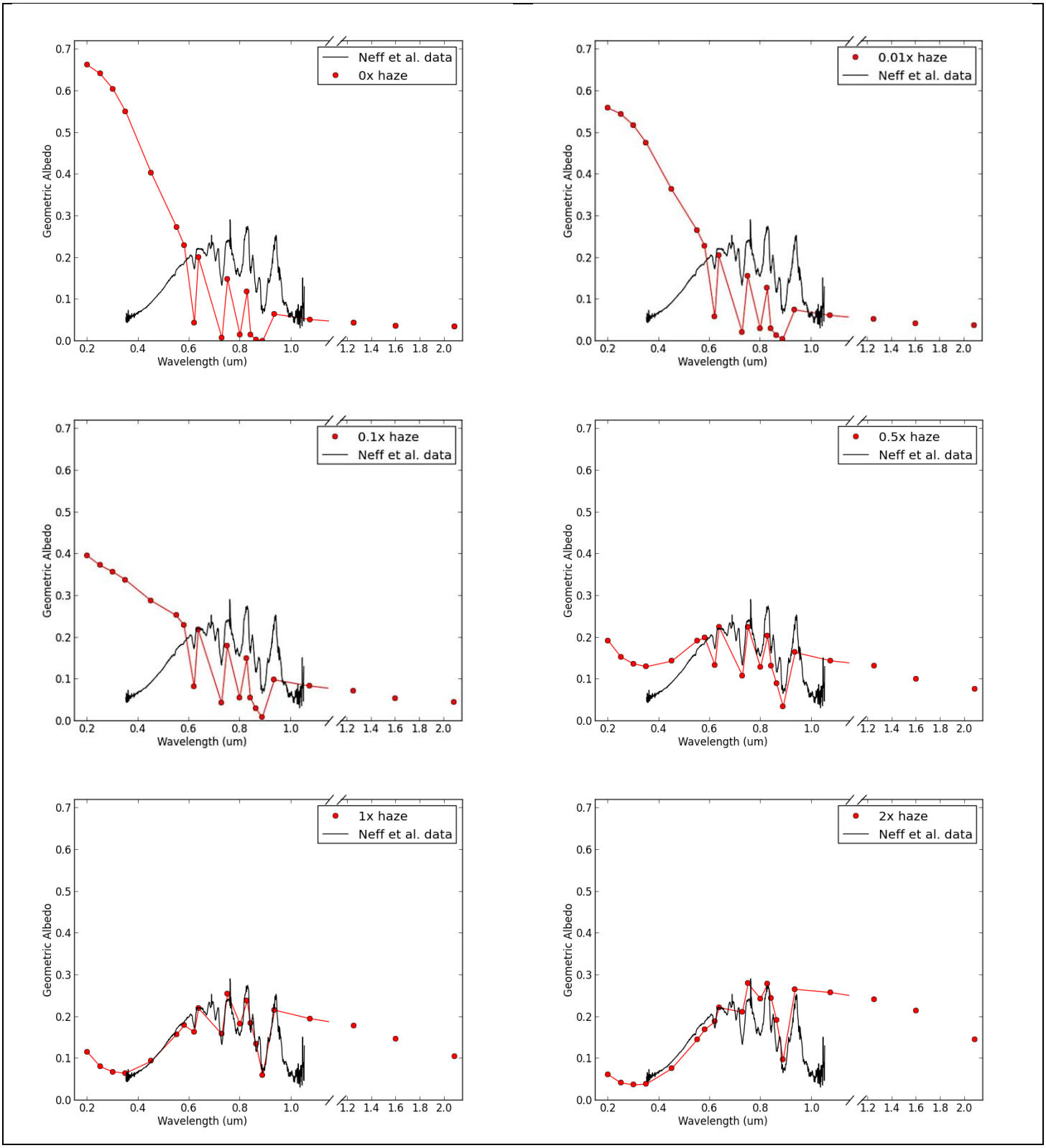

Figure 1. Geometric albedo spectra for several values of the haze production rate. All spectra are compared to data from Neff et al. (1984).

281

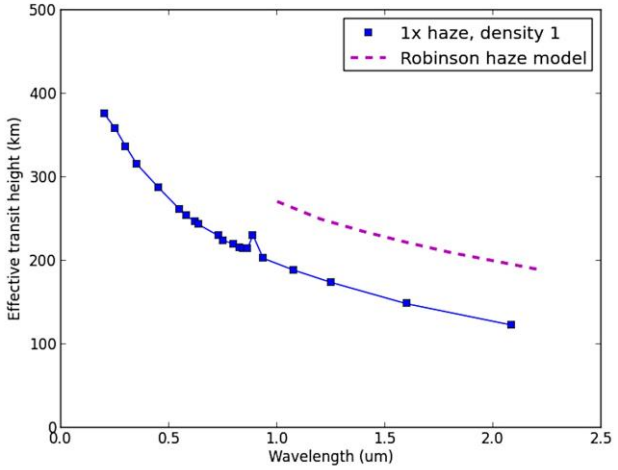

Figure 2. Comparison of effective transit height spectrum for the 1x Titan haze model to the effective transit height for present Titan determined by Robinson et al. (2014) in the continuum between the methane bands. The cutoff limb opacity is 0.56. The specific density of haze particles is 1.

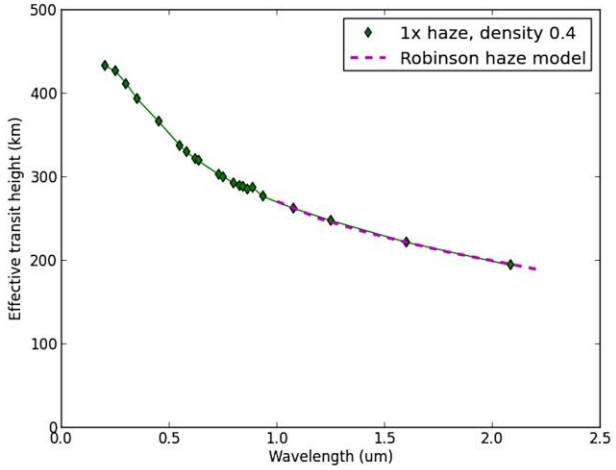

Figure 3. The same as Figure 2 but the bulk specific density of the haze particles reduced to 0.4 from the nominal value of 1.

Figures 2 and 3 present results for the effective transit height spectra with the 1x haze case, compared to results from Robinson et al. (2014**).** Note that the monotonic nature of the spectrum is a result of the relatively constant particle size over the range of transit heights. The model assumes that particles at a given altitude all have the same radius. Figure 3 of McKay et al. (1989) shows that for the nominal model, the particle size varies from 0.3 at 150 km to 0.1 at 350 km, which is the range of effective transit height studied here. The shape of the transit curve is consistent with that change. The particle size at 200 km varies with production rate; it is 0.19 um at 1x, 0.21 um at 2x and 0.13 um at 0.1x. When the particle density is decreased from 1 to 0.4, the particle size at 200 um increases to 0.3 um - as the particles descend more slowly and have more time to grow.

Robinson et al. used observations of solar occultations by Titan's atmosphere corrected for refraction effects from the Cassini mission, and fit a power law model of the haze to match the continuum points of the data. In Figure 2, we compare the effective transit height determined from our 1x Titan model for a limb optical depth of 0.56 and a specific density of haze particles of 1 to the continuum of Robinson et al. (2014). At 1 um, the altitude at which the limb optical depth reaches 0.56 is ~197 km, and two times the Chapman function at this altitude is 21.6. Hence the vertical optical depth corresponding to the limb is 0.026 – comparable to the vertical optical depth of 0.05 typically used to define the edge of a planet for the purpose of computing the geometric albedo from observations (Toon et al. 1992, Figure 18).

Our effective height at 1 um is about 70 km lower than determined by Robinson. If the specific density of the haze material is lowered to 0.4 (from 1), then the transit effective transit height fits the value of Robinson et al. (2014). This is shown in Figure 3. We note that the height at which the vertical optical depth of the haze reaches 0.5 in this modified model is 231 km and agrees with the tau value of 0.5 at 230 km inferred by Tomasko at al. (2009) from Huygens entry data.

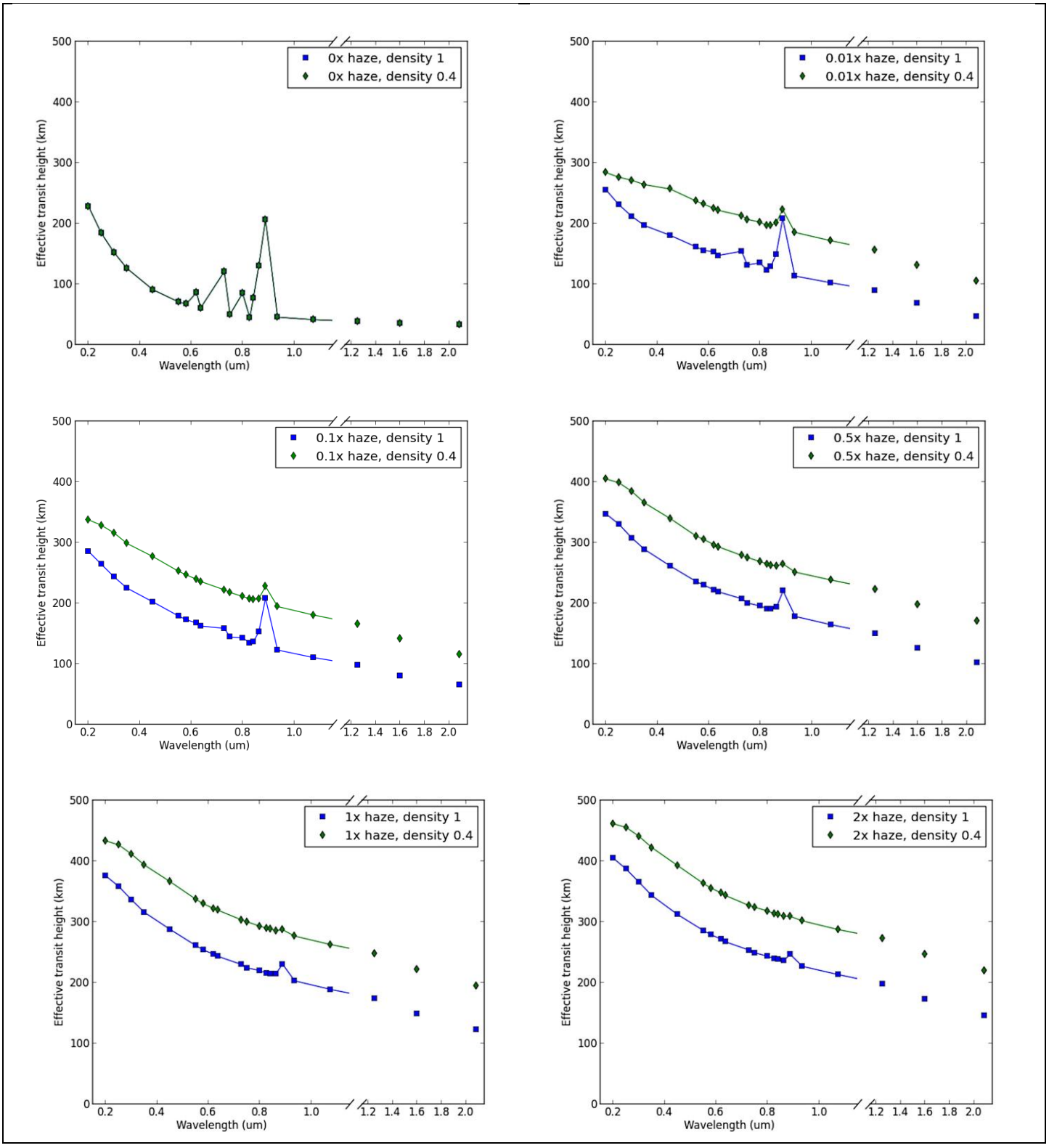

Figure 4. Effective transit height spectra for the 6 haze production rate values. The cutoff limb opacity is 0.56.

Figure 4 presents results for the effective transit height spectra of the six haze production rate cases: 0x, 0.01x, 0.1x, 0.5x, 1x, and 2x, with the cutoff limb opacity determined at 0.56 and with both cases of the specific density of the haze particles: 0.4 and 1. As mentioned above, the methane bands were modeled only in the visible range of wavelengths. In all cases, effective

transit height values decrease with increasing wavelength, with a steeper slope for smaller haze production rate values. As expected, the 0x haze case spectrum is unaffected by the values of the specific density of haze particles. For other haze cases, the effective transit heights increase for all wavelengths when reducing the specific density to 0.4.

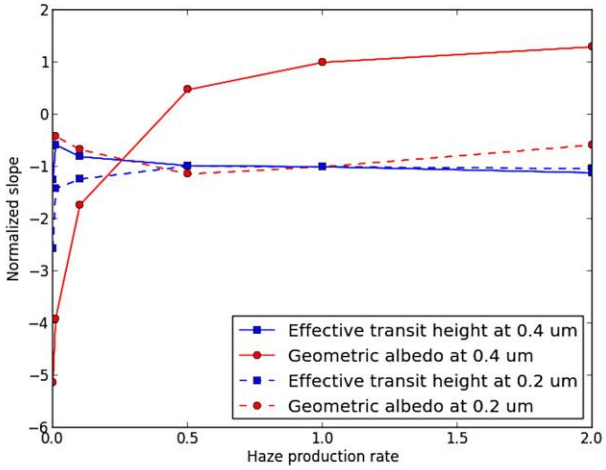

Figure 5. Slope of the geometric albedo and effective transit height spectra at 0.4 um and 0.2 um. The slope at 0.4 um is computed as (f(0.45 um) – f(0.35 um))/(0.1 um) where f is the value of the geometric albedo (Figure 1) or the effective transit height (Figure 4). For 0.2 um the slope is computed as (f(0.25 um) – f(0.2 um))/(0.05 um). Slope values are normalized at 1x production rate; to 1 for the geometric albedo and to -1 for the effective transit height. The specific density of the haze particles is 1.

Figure 5 shows the slopes at 0.4 um and 0.2 um of the geometric albedo and the transit height spectra. The values are normalized to 1 and -1 for the geometric albedo and the effective transit height, respectively. As can be seen in this figure, the slope of geometric albedo at 0.4 um changes clearly and smoothly as a function of haze production rate. All three other slopes (slope of the effective transit height at 0.2 um and 0.4 um and slope of the geometric albedo at 0.2 um) remain roughly constant. The slope of the effective transit height does show a sharp increase, but still small in magnitude, when increasing the haze from 0x to 0.01x.

4. DISCUSSION

In this section, we first analyze the geometric albedo spectra and consider how the spectra are affected by variations in the haze production rate for six values: 0x, 0.01x, 0.5x, 1x, 2x the present value characterizing Titan. Second, we compare our results of the effective transit height spectra for the 1x haze value with that of Robinson et al. (2014), and we analyze the changes observable in our spectra for our six haze production rates. Third, we analyze the change in slope with haze production rate for the geometric albedo and the effective transit height spectra.

4.1. Geometric albedo spectra

The six geometric albedo spectra (Figure 1) show that several spectral features are strongly affected by the value of the haze production rate. In the UV-visible range of wavelengths (0.2-0.6 um), the geometric albedo indicates whether the atmosphere is dominated by effects of the haze or Rayleigh scattering, which set a positive or negative slope respectively

(Courtin et al. 1991, McKay et al. 2001, Cahoy et al. 2010). When varying the haze production rate from 0x to 2x, the slope changes from blue (positive) to red (negative). A pure infinitely thick Rayleigh atmosphere has a geometric albedo of 0.75 (Dlugach and Yanovitskij 1974, Cahoy et al. 2010). Our results for zero haze approach this value at the shortest wavelengths but remain below 0.74 due to the fact that the atmosphere is not infinite and the surface is dark. The total column opacity due to Rayleigh scattering in the shortest wavelength (0.2 um) is 82.

In the visible-NIR range (0.6-1 um), the geometric albedo is affected by competing effects of the absorbing haze and the strong methane absorption bands (McKay et al. 1989, Coustenis et al. 1995). In the absence of haze, and due to the steep drop of Rayleigh scattering with increasing wavelength, methane absorption bands become prominent. When the haze is set to 1x or 2x, many of these bands become less prominent. It might have been expected that the haze production rate would correlate with amount of methane in the atmosphere (e.g., Sagan and Khare 1979, Khare et al. 1984, Sagan and Thompson 1984). However, as mentioned in section 3, the model varies the haze production rate separately from the amount of methane in the atmosphere. This is not unphysical, as both the amount of UV light and the amount of methane influence the haze production rate. A planet with very low UV light and methane could have only a very weak or no haze at all.

In the near-infrared (1-2 um), the haze becomes optically thin and less absorbing (Khare et al. 1984, McKay et al. 1991). As explained in section 2, we are interested in the 1-2 um range of wavelengths as a way to determine how the geometric albedo and effective transit height are sensitive to the lower atmosphere and surface. We thus did not add the methane bands in this range, similarly to the model of McKay et al. (1989). At these wavelengths, the geometric albedo is determined entirely by the surface albedo (McKay et al 1989). For a sphere with a Lambertian surface, the geometric albedo is 2/3 of the surface reflectance (Dlugach and Yanovitskij 1974, Sobolev 1975, Cahoy et al. 2010). In our results, the geometric albedo computed for zero haze approaches a constant value that is half this expected result. This is likely a result of the way that surface illumination is computed using a two-stream approximation, as discussed above. For a thick scattering atmosphere, the surface illumination is dominated by scattering, which is well represented in this model. But when the total optical depth becomes low, the albedo is just the sum of direct solar reflectance at all angles and this is not well represented in a two-stream calculation (Meador and Weaver 1979). When the optical depth goes to zero the geometric albedo is easily computed with no approximation, but to maintain consistency we did not alter the model to give the analytic result in this limit.

In comparing the geometric albedo for haze production rates from zero to twice the present rate on Titan, it is clear that the wavelength range from 0.2 to 0.6 um provides the most clear and direct indication of the haze production rate.

4.2. Effective transit height spectra

The effective transit height spectra also change in response to changes in the haze production rate. Two effective transit height spectra with a 1x haze production rate were computed and compared to the Robinson et al. (2014) result (Figures 2 and 3). We compare the continuum spectra; as for the 1x haze only one methane absorption band at 0.89 um is distinguishable. When keeping the specific density of haze particles at 1, our effective transit height spectrum does not agree closely with the Robinson haze model. Although the slopes of the models are very similar, our effective transit height values are slightly lower than Robinson et al.'s. At 1 um, our effective transit height is 200km while Robinson et al.'s is 271km. Robinson et al. do not model the haze at any lower wavelength than 1 um, which reduces possibilities for comparison. When reducing the specific density of the haze particles to 0.4, our spectrum

matches Robinson et al. well. The limb profile is sensitive to the properties of the haze in the optically thin region well above the main haze deck. The microphysics model of McKay et al. (1989) was developed based on fitting to the geometric albedo, which is sensitive to the properties of the main haze layer. In the upper regions of the atmosphere, McKay et al. assume that the particles were small spheres with density 1. Subsequent studies of the haze have shown that the haze forms fractal particles (reviewed in West et al., 2014) and as a result has a lower effective density and larger surface area. This causes the particles to fall slower in the atmosphere. We can approximate this effect in our model by reducing the density of the haze particles. If the specific density of the haze material is lowered to 0.4 (from 1) then the effective transit height fits the value of Robinson et al. (2014).

We then computed the effective transit height spectrum for each of the six values of the haze production rate (Figure 4). All spectra were computed for the two values of the specific density of the haze particles: 0.4 and 1. Overall, all effective transit height spectra show a decreasing height with increasing wavelength. In the 0.2 - 1 um wavelength range, the slope of the transit height changes sharply when increasing the haze production from 0x, and the sharp increase is largest for the shortest wavelength. This is due to the high absorption of the haze. However, the slope does not change significantly for haze production rates other than 0x. Another obvious difference between spectra of stronger hazes to spectra of weaker hazes is the value of the effective transit heights. Spectra with less amounts of hazes (0x, 0.01x, and 0.1x) have a much lower effective transit height than spectra of stronger hazes (1x and 2x), as expected. Although the haze is produced high in the atmosphere it becomes optically thick at much lower elevation, as the haze particles slow and coagulate in the denser lower atmosphere. When the haze production rate is decreased, the height at which the haze becomes dense enough to form an optically thick layer also decreases. A third difference is the prominence of methane absorption bands. The methane bands become more clearly visible as the haze is reduced – as was seen in the geometric albedo. It is important to note as mentioned above that the methane content of the atmosphere is constant in all cases. Reducing the specific density of the haze particles to 0.4 increases all values of the effective transit height. As expected, the 0x haze spectrum is unaffected. Effective transit heights of all other spectra are increased by about the same amount and methane bands are weakened such that they become barely visible in the 1x and 2x haze cases.

4.3. Slopes of spectra

Overall, the changes in the spectral features of the effective transit height spectra are less marked than the changes in the geometric albedo spectra when varying the haze production rate (Figures 1 and 3). The haze has a much stronger effect on the latter, especially in the UV-visible range of wavelengths. The overall shape of the effective transit height spectrum remains the same when varying the haze, with the difference being only a change of prominence of the methane absorption bands.

The slope of the effective transit height remains roughly constant, changing strongly only when completely removing the haze. The other haze cases have similar slopes, making it difficult to predict the production rate of haze in the atmosphere. The geometric albedo on the other hand has a clear change of slope at 0.4 um. This is clearly visible when looking at the slopes of both spectra at 0.4 um and 0.2 um (Figure 5). At 0.4 um, the slope of the geometric albedo spectrum increases with increasing haze production rate, going from negative for no haze to weak hazes (0x, 0.01x, and 0.1x) to positive for some haze to strong hazes (0.5x, 1x, and 2x). At 0.2 and 0.4 um, the slope of the effective transit height spectrum has a large onset when going from 0x to 0.01x, but remains close to constant for larger haze production rates. The slope of the geometric

albedo spectrum behaves similarly at 0.2 um. The slope of the geometric albedo at 0.4 um is thus a much clearer indicator of the haze production rate.

It is clear that the geometric albedo spectra provide more overall information than the effective transit height spectra. However, the effective transit height spectra probe the high elevation region of the atmosphere where the haze is optically thin, which is not well probed by the geometric albedo. Because of the minimum altitude at which effective transit height spectra probe, surface and tropospheric properties cannot be studied and only effects of the haze can be observed in a non-detailed manner. Overall, geometric albedo spectra are more affected by the presence of hazes, and provide a sensitive indicator of the surface and background gas properties.

5. CONCLUSIONS

We used the Titan haze model of McKay et al. (1989) to compute geometric albedo and effective transit height spectra as a function of haze production rate to consider how these can be used to characterize Titan-like exoplanets. From these results, we conclude that geometric albedo spectra are much more sensitive than effective transit height spectra to the haze production rate and the background Rayleigh gas.

When varying the haze production rate from 0x to 2x the value characterizing Titan, the slope of the geometric albedo profile changes greatly in the UV-visible range, going from negative (blue) to positive (red). This indicates a change from a Rayleigh-dominated atmosphere to a haze-dominated atmosphere. This spectral region is the most effective way to determine the presence of a thick haze from remote observations.

In contrast, when varying the haze production rate from 0x to 2x, the same overall shape of the effective transit height spectrum persists, decreasing smoothly with increasing wavelength. A noticeable change was a large slope onset when increasing the haze production rate from 0x to 0.01x, but the slope remained close to constant for all other haze production rates. The methane absorption bands became more prominent for weaker hazes. The lowest altitude probed by the effective transit height spectra is 34 km, making it insensitive to changes in surface properties such as the surface albedo.

While transit spectroscopy of distant exoplanets is well underway, our results suggest that important and complementary information can be obtained from the geometric albedo and motivates improvements in the technology for direct imaging of nearby exoplanets.

6. ACKNOWLEDGMENTS

We thank our two reviewers for their comments, which greatly improved the clarity of the paper. Support from NASA Exoplanets Research Program and NASA's Nexus for Exoplanet Systems Science (NExSS) program is acknowledged.

APPENDIX

The Chapman function allows us to compute the limb optical depth for an atmosphere given the vertical optical depth computed at a fixed altitude.

By definition,

$$\tau(h_P) = 2\,\tau_V(h_P)\,Ch\left(X_P,\ \theta_P = \frac{\pi}{2}\right) \quad \text{(A.1)}$$

where h_P is the altitude at the closest point P to the surface of the planet, and $X_P = r_P/H(at\ h = h_P)$ with $r_P = R + h_P$, R being the radius of the planet and $H(h = h_P)$ is the scale height at altitude h_P. θ_P is the stellar zenith angle at point P, here it is fixed at $\pi/2$. τ_V is the vertical optical depth at h_P. $\tau(h_P)$ is the limb optical depth along a slant path passing through point P at h_P.

The Chapman function is defined as the ratio of the horizontal integrated density (N_H) to the vertical integrated density (N_V).

$$Ch(X_p, \theta_p) = N_H/N_V \quad \text{(A.2)}$$

Assuming an exponentially distributed atmosphere the concentration at altitude h is defined as

$$n(h) = n_0 \exp[-h/H(h)] \quad \text{(A.3)}$$

Symbols used in equations (1), (2), (3), and in the subsequent discussion are as follow:

- h — Altitude, $h = h_P\ at\ point\ P$
- n — Concentration of the atmospheric constituent, $n = n_P\ at\ point\ P, n = n_0\ at\ h = 0$
- H — Scale height
- R — Radius of planet or moon of interest
- r_P — Radial distance to point P: $r_P = R + h_P$
- X_P — $= r_P/H$
- θ_P — Stellar zenith angle at point P
- s — Distance coordinate along the line of sight, measured towards the star from $s = s_P$ at point P to the horizon $s = \infty$

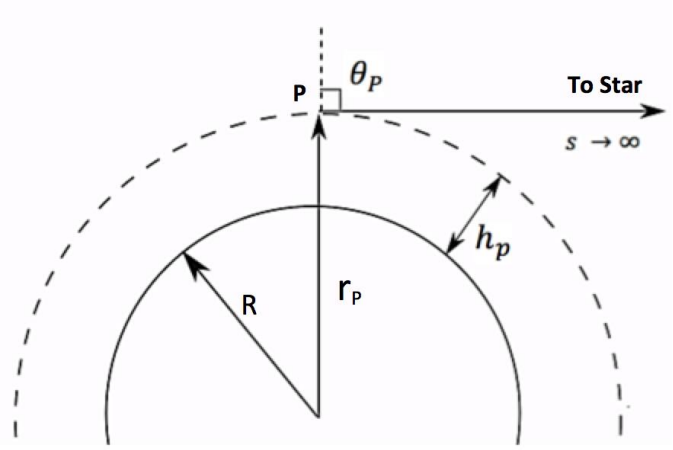

Figure A.1. Geometry for $\theta_p = \frac{\pi}{2}$

The vertical integrated column density of the atmosphere above a point P at altitude h_P is

$$N_V = \int_{h_p}^{\infty} n\, dh \tag{A.4}$$

Because the scale height H depends on h, it is better to keep N_V in its integral form and compute it. This differs from papers on the Chapman function and subsequent papers, which used the function by assuming a constant scale height for all altitudes.

Thus,

$$N_V = n_0 \int_{h_p}^{\infty} \exp[-h/H(h)]\ dh \tag{A.5}$$

Similarly, the horizontal integrated density from point s_P to horizon along the line of sight is expressed as

$$N_H = n_0 \int_{s_p}^{\infty} \exp[-h/H(h)]\ ds \tag{A.6}$$

From trigonometry we can see from figure A.1 that

$$ds = \sec\theta\ dh \tag{A.7}$$

and

$$\frac{\sin\theta_p}{h+R} = \frac{\sin\theta}{h_p+R} \tag{A.8}$$

Taking the square of both sides and rearranging

$$\sin^2\theta = \left(\frac{h_p+R}{h+R}\right)^2 \sin^2\theta_p \tag{A.9}$$

With some algebra and because $\cos^2\theta = 1 - \sin^2\theta$,

$$\cos^2\theta = 1 - \left[\left(\frac{h_p+R}{h+R}\right)^2 \sin^2\theta_p\right] \tag{A.10}$$

Using the fact that $\frac{1}{\cos^2\theta} = \sec^2\theta$ and rearranging for $\sec\theta$

$$\sec\theta = \frac{[(h+R)/r_P]}{[[(h+R)/r_P]^2 - \sin^2\theta_P]^{1/2}} \tag{A.11}$$

Substituting this expression for $\sec\theta$ into the expression for ds

$$ds = \frac{[(h+R)/r_P]}{[[(h+R)/r_P]^2 - \sin^2\theta_P]^{1/2}}\ dh \tag{A.12}$$

Putting this into the integral for N_H and changing the limits of integration accordingly we have

$$N_H = n_0 \int_{h_p}^{\infty} \exp[-h/H(h)]\ \frac{[(h+R)/r_P]}{[[(h+R)/r_P]^2 - \sin^2\theta_P]^{1/2}}\ dh \tag{A.13}$$

Thus using our two expressions for N_V and N_H, we express the Chapman function as

$$Ch(X_p, \theta_p) = \frac{\int_{h_p}^{\infty} \exp[-h/H(h)]\ \frac{[(h+R)/r_P]}{\left[[(h+R)/r_P]^2 - \sin^2\theta_P\right]^{1/2}}\, dh}{\int_{h_p}^{\infty} \exp[-h/H(h)]\ dh} \tag{A.14}$$

This expression has as its only assumption an exponentially distributed atmosphere and can be computed easily by modern computing methods.

In our case, we want to compute the Chapman function for $\theta_p = \frac{\pi}{2}$, thus the function can be reduced to

$$Ch\left(X_p, \frac{\pi}{2}\right) = \frac{\int_{h_p}^{\infty} \exp[-h/H(h)]\ \frac{[(h+R)/r_P]}{\left[[(h+R)/r_P]^2 - 1\right]^{1/2}}\, dh}{\int_{h_p}^{\infty} \exp[-h/H(h)]\ dh} \tag{A.15}$$

This is the formulation that has been used in this paper, with no further approximation.

In order to further reduce this expression, previous papers including Smith and Smith (1972) have assumed that the atmosphere can be approximated as having a constant scale height at all altitudes. This approximation allows us to reduce equation (A.15) into a form that often appears in literature where the Chapman function is computed. It is thus interesting to perform this approximation ourselves.

If this approximation is made, integrating N_V gives

$$N_V = n_P H \tag{A.16}$$

with $n_P = n_0 \exp[-h_P/H]$.

And so

$$Ch(X_p, \theta_p) = \frac{\exp[h_P/H]}{H} \int_{h_P}^{\infty} \exp[-h/H] \ \frac{[(h+R)/r_P]}{[[(h+R)/r_P]^2 - \sin^2\theta_P]^{1/2}} \ dh \tag{A.17}$$

It is now possible to approximate this expression in the case where $r_p \gg H$. For that purpose, it is helpful to first substitute $u = h - h_p$ into equation (A.17).

We thus have

$$Ch(X_p, \theta_p) = \frac{\exp[h_P/H]}{H} \int_0^{\infty} \exp[-(u + h_P)/H] \ \frac{[1+(u/r_P)]}{\left[[1+(u/r_P)]^2 - \sin^2\theta_p\right]^{1/2}} \ du \tag{A.18}$$

If $r_p \gg H$, we can neglect u/r_P in the numerator and $(u/r_P)^2$ in the denominator:

$$Ch(X_p, \theta_p) = \frac{\exp[h_P/H]}{H} \int_0^{\infty} \exp[-(u + h_P)/H] \frac{1}{\left[\ (2u/r_P) + \cos^2\theta_p\right]^{1/2}} \ \square u \tag{A.19}$$

and further

$$Ch(X_p, \theta_p) = \frac{1}{H} \int_0^{\infty} \exp[-u/H] \frac{1}{\left[\frac{2u}{r_p} + \cos^2\theta_p\right]^{1/2}} \ du \tag{A.20}$$

which differs from Smith and Smith (1972) only by the fact that they left the extra term $e^{\frac{h_p}{H}}$ in front of the integral, but they corrected this error in subsequent equations.

With no further approximation, equation (A.20) can be rewritten as

$$Ch(X_p, \theta_p) = \left[\frac{\pi}{2} X_p\right]^{1/2} \exp[y^2] \, erfc(y) \tag{A.21}$$

with $y = (X_P/2)^{1/2} \left|\cos\theta_p\right|$. This expression is similarly obtained by Smith and Smith (1972).

In our case, $\theta_p = \frac{\pi}{2}$, and so

$$Ch\left(X_p, \frac{\pi}{2}\right) = \left[\frac{\pi}{2} X_p\right]^{1/2} \tag{A.22}$$

This expression assumes three facts: an exponentially distributed atmosphere, a constant scale height at all altitudes, and $r_p \gg H$ for the planet of interest.

It is important to judge how valid this approximation is before deciding to use it as the Chapman function. Smith and Smith (1972) have measured the difference in the two approximated Chapman functions, (A.18) and (A.24), for different values of r_p/H. Both those expressions assume an exponentially distributed atmosphere and a constant scale height. (A.21) further assumes $r_p \gg H$. We note that since (A.18) already makes the approximation of a constant scale height, we can expect our formulation of the Chapman (A.15), with a scale height dependent on altitude, to be the most accurate.

For a planet of interest, r_p/H can be approximated as

$$\frac{r_p}{H} = \frac{R+h}{H} = \frac{R}{H} + \frac{h}{H} \approx \frac{R}{H} \tag{A.23}$$

for any altitude h.

For $\theta_p = \frac{\pi}{2}$, if $\frac{r_p}{H} \geq 500$, Smith and Smith (1972) have measured that the difference between (A.21) and (A.18) is very small ($\leq 0.1\%$), but that if $\frac{r_p}{H} \leq 50$, it becomes non-negligible ($\geq 1\%$). For the Earth and Venus, $\frac{r_p}{H} \approx 1000$, and the approximated form of the Chapman function (A.24) can thus be used without causing the calculations to differ much. However, for Titan, $\frac{r_p}{H} \approx 20$, and the Chapman expression (A.18) will give more accurate values. We can expect that using the complete form of the complete Chapman (A.15), with a scale height dependent on altitude, will allow for the most accurate results in our computations.

We build on this analysis by focusing on $\theta_p = \frac{\pi}{2}$ and investigating the difference between the approximated (A.22, A.21 with $\theta_p = \frac{\pi}{2}$) and the complete Chapman function (A.15) (non-constant scale height) as a function of altitude, for Earth and Titan. The validity of the approximation in (A.22) depends not only on the size of the planet but also varies with elevation both explicitly and through changes in the scale height with elevation.

For the Earth, we used the temperature profile up to 85 km as in the U.S. Standard Atmosphere (1976) and computed the complete Chapman function as well as its approximate form. For Titan, we used the temperature values from McKay et al. (1989) and computed the Chapman function and its approximate form for altitudes up to 657 km.

Table 3. Difference (%) between full Chapman and approximated Chapman functions

Earth		Titan	
Altitude (km)	**Difference (%)**	**Altitude (km)**	**Difference (%)**
0-10	0.04-0.05	0-110	6-12
11-33	0.03-0.04	111-449	0.2-6
34-64	0.04-0.05	450-657	6-12
65-85	0.03-0.04		

Table 3 indicates the appropriate use of the approximate form for the Chapman function (A.22) when computing the function for Earth-like planets, as the difference between the complete and the approximate form is always below 1%. However, the difference is much larger when computing the function for Titan. Using the approximate form of the Chapman will negatively affect the accuracy of the limb optical depths we compute, and subsequently the effective transit heights. We conclude that the complete form of the Chapman function (A.15) should be used when studying the atmospheres of Titan-like planets.

REFERENCES

Bean, J., Kempton, E., Homeier, D. (2010). A ground-based transmission spectrum of the super-Earth exoplanet GJ 1214b. Nature 468, 669-672.

Bellucci, A., Sicardy, B., Drossart, P., Rannou, P., Nicholson, P.D., Hedman, M., Baines, K.H., Burrati, B. (2009). Titan solar occultation observed by Cassini/VIMS: Gas absorption and constraints on aerosol composition. Icarus 201, 198-216.

Betremieux, Y., Kaltenegger, L. (2014). Impact Of Atmospheric Refraction: How Deeply Can We Probe Exo-Earth's Atmospheres During Primary Eclipse Observations? ApJ The Astrophysical Journal 791, 7-7.

Brown, T. (2001). Transmission Spectra as Diagnostics of Extrasolar Giant Planet Atmospheres. ApJ The Astrophysical Journal 553, 1006-1026.

Cable et al. Titan Tholins: Simulating Titan Organic Chemistry in the Cassini-Huygens Era. Chemical Reviews (2011)

Cahoy, K., Marley, M., Fortney, J. (2010). Exoplanet albedo spectra and colors as a function of planet phase, separation, and metallicity. ApJ The Astrophysical Journal 724, 189-214.

Chapman, S. (1931). The absorption and dissociative or ionizing effect of monochromatic radiation in an atmosphere on a rotating earth part II. Grazing incidence. Proc. Phys. Soc. Proceedings of the Physical Society 43, 483-501.

Coll et al. Experimental laboratory simulation of Titan's atmosphere: aerosols and gas phase. Planet Space Sci (1999) vol. 47 pp. 1331-1340

Courtin, R., Wagener, R., Mckay, C.P., Caldwell, J., Fricke, K., Raulin, F., Bruston, P. (1991). UV spectroscopy of Titan's atmosphere, planetary organic chemistry and prebiological synthesis. Icarus 90, 43-56.

Coustenis, A., Lellouch, E., Maillard, J., Mckay, C. (1995). Titan's Surface: Composition and Variability from the Near-Infrared Albedo. Icarus 118, 87-104.

de Kok, R., Stam, D. (2012). The influence of forward-scattered light in transmission measurements of (exo)planetary atmospheres. Icarus 221, 517-524.

Dlugach, J., Yanovitskij, E. (1974). The optical properties of Venus and the Jovian planets. II. Methods and results of calculations of the intensity of radiation diffusely reflected from semi-infinite homogeneous atmospheres. Icarus 22, 66-81.

Elachi, C. (2005). Cassini Radar Views the Surface of Titan. Science 308, 970-974.

Fortney, J. (2005). The effect of condensates on the characterization of transiting planet atmospheres with transmission spectroscopy. Monthly Notices of the Royal Astronomical Society 364, 649-653.

Fulchignoni, M., Ferri, F., Angrilli, F., Ball, A.J., Bar-Nun, A., Barucci, M. A., Bettanini, C., Bianchini, G., Borucki, W., Colombatti, G., Coradini, M., Coustenis, A., Debei, S., Falkner, P., Fanti, G., Flamini, E., Gaborit, V., Grard, R., Hamelin M., Harri, A.M., Hathi, B., Jernej, I., Leese, M.R., Lehto, A., Lion Stoppato, P.F., López-Moreno, J.J., Mäkinen, T., McDonnel, J.A.M., McKay, C.P., Molina-Cuberos, G., Neubauer, F.M., Pirronello, V., Rodrigo, R., Saggin, B., Schwingenschuh, K., Seiff, A., Simões, F., Svedhem, H., Tokano, T., Towner, M.C., Trautner, R., Withers, P., Zarnecki., J.C. (2005). In situ measurements of the physical characteristics of Titan’s environment. Nature 438, 785–791.

Gibson, N., Pont, F., Aigrain, S. (2011). A new look at NICMOS transmission spectroscopy of HD 189733, GJ-436 and XO-1: No conclusive evidence for molecular features. Monthly Notices of the Royal Astronomical Society 451, 2199-2213.

Hubbard, W., Fortney, J., Lunine, J., Burrows, A., Sudarsky, D., & Pinto, P. (2001). Theory of Extrasolar Giant Planet Transits. ApJ The Astrophysical Journal 560, 413-419.

Imanaka, H., Khare, B., Elsila, J., Bakes, E., Mckay, C.P., Cruikshank, D., Sugita, S., Matsui, T., Zare, R. (2004). Laboratory experiments of Titan tholin formed in cold plasma at various pressures: Implications for nitrogen-containing polycyclic aromatic compounds in Titan haze. Icarus 168, 344-366.

Ingraham, P., Marley, M., Saumon, D., Marois, C., Macintosh, B., Barman, T., Bauman, B. Burrows, A., Chilcote, J.K., 8, De Rosa, R.J., Dillon, D., Doyon, R., Dunn, J.,Erikson, D., Fitzgerald, M.P., Gavel, D., Goodsell, S.J., Graham, J.R., Hartung, M., Hibon, P., Kalas, P.G., Konopacky, Q., Larkin, J.A., Maire, J., Marchis, F., McBride, J., Millar-Blanchaer, M., Morzinski, K.M., Norton, A., Oppenheimer, R., Palmer, D.W., Patience, J., Perrin, M.D., Poyneer, L.A., Pueyo, L., Rantakyrö, F., Sadakuni, N., Saddlemyer, L., Savransky, D., Soummer, R., Sivaramakrishnan, A., Song, I., Thomas, S., Wallace, K., Wiktorowicz, S.J., Wolff, S.G. (2014). Gemini Planet Imager Spectroscopy of the HR 8799 Planets c and d. The Astrophysical Journal Letters 794, L15.

Karkoschka, E. (1994) Spectrophotometry of the Jovian Planets and Titan at 300- to 1000-nm Wavelength: The Methane Spectrum. Icarus 111, 174-192.

Khare, B.N., Sagan, C., Arakawa, E.T., Suits, F., Callcott, T.A., Williams, M.W. (1984). Optical constants of organic tholins produced in a simulated Titanian atmosphere: from soft X-ray to microwave frequencies. Icarus 60, 127–137.

Kunde, V., Aikin, A., Hanel, R., Jennings, D., Maguire, W., Samuelson, R. (1981). C4H2, HC3N and C2N2 in Titan's atmosphere. Nature 292, 686-688.

Lara, L.M., Lorenz, R.D., Rodrigo, R. (1994). Liquids and solids on the surface of Titan. Planetary and Space Science 42, 5–14.

Lavvas et al. Coupling photochemistry with haze formation in Titan's atmosphere, Part II: Results and validation with Cassini/Huygens data. Planet Space Sci (2008) vol. 56 (1) pp. 67-99

Lecavalier des Etangs, A., Pont, F., Vidal-Madjar, A., Sing, D. (2008). Rayleigh scattering in the transit spectrum of HD 189733b. Astronomy and Astrophysics A&A 481. 83-86.

Lorenz, R., Lunine, J. (1997). Titan's surface reviewed: the nature of bright and dark terrain. Icarus 45, 981-992.

Lorenz, R., Lunine, J. (2005). Titan's surface before Cassini. Planetary and Space Science 53, 557-576.

Lorenz, R. (2006). The sand seas of Titan: Cassini RADAR observations of longitudinal dunes. Science 312, 724-727.

Lunine, J.I. (2009). Saturn's Titan: a strict test for life's cosmic ubiquity. Proceedings of the American Philosophical Society 153, 403–418.

Macintosh, B., J. R. Graham, T. Barman, R. J. De Rosa, Q. Konopacky, M. S. Marley, C. Marois, E. L. Nielsen, L. Pueyo, A. Rajan, J. Rameau, D. Saumon, J. J. Wang, J. Patience, M. Ammons, P. Arriaga, E. Artigau, S. Beckwith, J. Brewster, S. Bruzzone, J. Bulger, B. Burningham, A. S. Burrows, C. Chen, E. Chiang, J. K. Chilcote, R. I. Dawson, R. Dong, R. Doyon, Z. H. Draper, G. Duchene, T. M. Esposito, D. Fabrycky, M. P. Fitzgerald, K. B. Follette, J. J. Fortney, B. Gerard, S. Goodsell, A. Z. Greenbaum, P. Hibon, S. Hinkley, T. H. Cotten, L.-W. Hung, P. Ingraham, M. Johnson-Groh, P. Kalas, D. Lafreniere, J. E. Larkin, J. Lee, M. Line, D. Long, J. Maire, F. Marchis, B. C. Matthews, C. E. Max, S. Metchev, M. A. Millar-Blanchaer, T. Mittal, C. V. Morley, K. M. Morzinski, R. Murray-Clay, R. Oppenheimer, D. W. Palmer, R. Patel, M. D. Perrin, L. A. Poyneer, R. R. Rafikov, F. T. Rantakyro, E. L. Rice, P. Rojo, A. R. Rudy, J.- B. Ruffio, M. T. Ruiz, N. Sadakuni, L. Saddlemyer, M. Salama, D. Savransky, A. C. Schneider, A. Sivaramakrishnan, I. Song, R. Soummer, S. Thomas, G. Vasisht, J. K. Wallace, K. Ward-Duong, S. J. Wiktorowicz, S. G. Wolff, and B. Zuckerman. (2015). Discovery and Spectroscopy of the Young Jovian Planet 51 Eri B with the Gemini Planet Imager. (2015). Discovery and spectroscopy of the young jovian planet 51 Eri b with the Gemini Planet Imager. Science 350(6256), 64-67.

Marley, M., Gelino, C., Stephens, D., Lunine, J., Freedman, R. (1999). Reflected Spectra and Albedos of Extrasolar Giant Planets. I. Clear and Cloudy Atmospheres. ApJ The Astrophysical Journal 513, 879-893.

McKay, C.P., Pollack, J.B., Courtin, R. (1989). The thermal structure of Titan's atmosphere. Icarus 80, 23–53.

McKay, C.P., Pollack, J.B., Courtin, R. (1991). The greenhouse and antigreenhouse effects on Titan. Science 253, 1118–1121.

McKay, C.P. (1996). Elemental composition, solubility, and optical properties of Titan's organic haze. Planetary and Space Scence 44, 741-747.

McKay, C.P., Coustenis, A., Samuelson, R.E., Lemmon, M.T., Lorenz, R.D., Cabane, M., Rannou, P., Drossart, P. (2001). Physical properties of the organic aerosols and clouds on Titan. Planetary and Space Science 49, 79–99.

Meador, W. E., & Weaver, W. R. (1980). Two-stream approximations to radiative transfer in planetary atmospheres: A unified description of existing methods and a new improvement. Journal of the Atmospheric Sciences, 37(3), 630-643.

Mesa, D., R. Gratton, A. Zurlo, A. Vigan, R. U. Claudi, M. Alberi, J. Antichi, A. Baruffolo, J.-L. Beuzit, A. Boccaletti, M. Bonnefoy, A. Costille, S. Desidera, K. Dohlen, D. Fantinel, M. Feldt, T. Fusco, E. Giro, T. Henning, M. Kasper, M. Langlois, A.-L. Maire, P. Martinez, O. Moeller-Nilsson, D. Mouillet, C. Moutou, A. Pavlov, P. Puget, B. Salasnich, J.-F. Sauvage, E. Sissa, M. Turatto, S. Udry, F. Vakili, R. Waters, and F. Wildi. (2015). Performance of the VLT Planet Finder SPHERE. Astronomy & Astrophysics, 576: A121.

Misra, A., Meadows, V., & Crisp, D. (2014). The Effects of Refraction on Transit Transmission Spectroscopy: Application to Earth-like Exoplanets. The Astrophysical Journal, 792(1), 61.

Neff, J., Humm, D., Bergstralh, J., Cochran, A., Cochran, W., Barker, E., Tull, R. (1984). Absolute spectrophotometry of Titan, Uranus, and Neptune: 30,500–10,500 Å. Icarus 60, 221-235.

Niemann, H. B., Atreya, S. K., Bauer, S. J., Carignan, G. R., Demick, J. E., Frost, R. L., Gautier, D., Haberman, J.A., Harpold, D. N., Huntern, D. M., Israel, G., Lunine, J. I., Kasprzak, W. T., Owen, T. C., Paulkovich, M., Raulin, F., Raaen, E., Way, S. H. (2005). The abundances of constituents of Titan's atmosphere from the GCMS instrument on the Huygens probe. Nature, 438(7069), 779-784.

Pont, F., Knutson, H., Gilliland, R., Moutou, C., Charbonneau, D. (2008). Detection of atmospheric haze on an extrasolar planet: The 0.55-1.05 μm transmission spectrum of HD 189733b with the Hubble Space Telescope. Monthly Notices of the Royal Astronomical Society 451, 109-118.

Porco, C.,Baker, E., John Barbara, Kevin Beurle, Andre Brahic, Joseph A. Burns, Sebastien Charnoz, Nick Cooper, Douglas D. Dawson, Anthony D. Del Genio, Tilmann Denk, Luke Dones, Ulyana Dyudina, Michael W. Evans, Stephanie Fussner, Bernd Giese, Kevin Grazier, Paul Helfenstein, Andrew P. Ingersoll, Robert A. Jacobson, Torrence V. Johnson, Alfred McEwen, Carl D. Murray, Gerhard Neukum, William M. Owen, Jason Perry, Thomas Roatsch, Joseph Spitale, Steven Squyres, Peter Thomas, Matthew Tiscareno, Elizabeth P. Turtle, Ashwin R. Vasavada, Joseph Veverka, Roland Wagner, Robert West. (2005). Imaging of Titan from the Cassini spacecraft. Nature 434, 159-168.

Radebaugh, J., Lorenz, R., Kirk, R., Lunine, J., Stofan, E., Lopes, R., Wall, S. (2007). Mountains on Titan observed by Cassini Radar. Icarus 192, 77-91.

Rages, K., Pollack, J. (1980). Titan aerosols: Optical properties and vertical distribution. Icarus 41, 119-130.

Rages, K., Pollack, J., Smith, P. (1983). Size estimates of Titan's aerosols based on Voyager high-phase-angle images. J. Geophys. Res. Journal of Geophysical Research 88, 8721-8721.

Rannou, P., Cours, T., Le Mouélic, S., Rodriguez, S., Sotin, C., Drossart, P., Brown, R. (2010). Titan haze distribution and optical properties retrieved from recent observations. Icarus 208. 850-867.

Robinson, T., Maltagliati, L., Marley, M., Fortney, J. (2014). Titan solar occultation observations reveal transit spectra of a hazy world. Proceedings of the National Academy of Sciences 111, 9042-9047.

Seager, S., Sasselov, D. (2000). Theoretical Transmission Spectra during Extrasolar Giant Planet Transits. ApJ The Astrophysical Journal 537, 916-921.

827 Sing, D., Désert, J., Lecavalier des Etangs, A., Ballester, G., Vidal-Madjar, A., Parmentier, V.,
828 Hebrard, G., Henry, G. (2009). Transit spectrophotometry of the exoplanet HD 189733b. A&A
829 Astronomy and Astrophysics 505. 891-899.
830
831 Smith, F., Smith, C. (1972). Numerical evaluation of Chapman's grazing incidence integral ch
832 (X, χ). J. Geophys. Res. Journal of Geophysical Research 77, 3592-3597.
833
834 Sobolev, V. (1975). Light Scattering in Planetary Atmospheres, International Series of
835 Monographs in Natural Philosophy 76, 52-73.
836
837 Szopa et al. PAMPRE: A dusty plasma experiment for Titan's tholins production and study.
838 Planet Space Sci (2006) vol. 54 (4) pp. 394-404
839
840 Tomasko, M.G. and West, R. A. (2009), Aerosols in Titan's Atmosphere, Titan from Cassini-
841 Huygens, Eds. Brown R.H., Lebreton, J-P., Waite, J. H., Springer, pp.297-321.
842
843 Toon, O., Turco, R., Jordan, J., Goodman, J., Ferry, G. (1989). Physical processes in polar
844 stratospheric ice clouds. J. Geophys. Res. Journal of Geophysical Research 94, 11359-11380.
845
846 Toon, O. B., McKay, C. P., Griffith, C. A., & Turco, R. P. (1992). A physical model of Titan's
847 aerosols. Icarus, 95(1), 24-53.
848
849 Vidal-Madjar, A., Arnold, L., Ehrenreich, D., Ferlet, R., Lecavalier des Etangs, A., Bouchy, F.,
850 Segransan, D., Boisse, I., Hebrard, G., Moutou, C., Desert, J., Sing, D., Cabanac, R., Nitschelm,
851 C., Bonfils, X., Delfosse, X., Desort, M., Diaz, R., Eggenberger, A., Forveille, T., Lagrange, A.,
852 Lovis, C., Pepe, F., Perrier, C., Pont, F., Santos, N., Udry, S. (2010). The Earth as an extrasolar
853 transiting planet. A&A Astronomy & Astrophysics 523, A57.
854
855 West, R., Lavvas, P., Anderson, C., **Imanaka, H.**, Titan Haze, in "Titan: Surface, Atmosphere
856 and Magnetosphere", Edited by Mueller-Wodarg, I., Griffith, C., Lellouch, E., Cravens,
857 T., Cambridge University Press, 2014, p. 285-321.
858
859
860 Wilson and Atreya. Current state of modeling the photochemistry of Titan's mutually dependent
861 atmosphere and ionosphere. J Geophys Res-Planet (2004) vol. 109 (E6) pp. E06002
862
863 Wolf, E. T., Toon, O. B. (2010). Fractal organic hazes provided an ultraviolet shield for early
864 Earth. Science, 328(5983), 1266-1268.
865
866 Yung, Y.L., Allen, M., Pinto, J.P. (1984). Photochemistry of the atmosphere of Titan:
867 comparison between model and observations. ApJS The Astrophysical Journal Supplement
868 Series 55, 465–506.
869